Journal of Power Sources 201 (2012) 81–87

Contents lists available at SciVerse ScienceDirect

Journal of Power Sources

journal homepage: www.elsevier.com/locate/jpowsour

Facile synthesis of poly(amidoamine)-modified carbon nanospheres supported Pt nanoparticles for direct methanol fuel cells

Yingqiang Huang[a], Haoliang Huang[a], Yingju Liu[a,*], Yan Xie[a], Zhurong Liang[a], Chuanhe Liu[b]

[a] Institute of Biomaterials, Department of Applied Chemistry, College of Sciences, South China Agricultural University, Guangzhou 510642, China
[b] Instrumental Analysis & Research Center, South China Agricultural University, Guangzhou 510642, China

ARTICLE INFO

Article history:
Received 1 October 2011
Received in revised form 28 October 2011
Accepted 31 October 2011
Available online 6 November 2011

Keywords:
Poly(amidoamine)
Hydrothermal
Carbon nanospheres
Direct methanol fuel cell
Electrocatalyst

ABSTRACT

In this work, the synthesis and characterization of a catalyst material consisted of Pt, poly(amidoamine) (PAMAM) and carbon nanospheres are investigated. Firstly, carbon nanospheres are hydrothermally synthesized, followed by a high temperature of calcination to achieve a high amount of oxygen-containing groups. Subsequently, these carbon nanospheres are modified with multifunctional PAMAM dendrimers to form coordinate complex with H_2PtCl_6, followed by the reduction with sodium borohydride to obtain metallic Pt. The resulting composites are characterized by transmission electron microscopy (TEM), X-ray photoelectron spectroscopy (XPS) and infrared spectroscopy (IR). This new nanomaterial is used as catalysts for methanol electro-oxidation and their electrochemical features are investigated in detail by cyclic voltammetry, chronoamperometry and CO-stripping analysis. The results of this study suggest that, through modification with multifunctional dendrimers, complex carbon nanospheres-based materials can be fabricated, where Pt nanoparticles are smaller, more abundant and more uniformly distributed, thereby providing higher electrocatalytic ability in direct methanol fuel cell and many possibilities for various applications in biosensors and biomedical diagnosis.

1. Introduction

The direct methanol fuel cell (DMFC) is considered to be a promising energy conversion device for future energy-generating devices, especially for mobile and portable applications, due to its high energy density, simplicity and fast recharging [1,2]. However, there are still some troubles that must face before its commercial utilization, including the rapid poison by the adsorption of CO produced during the oxidation of methanol and the scare supply of Pt [3]. It is well known that some Pt-based alloy or Pt-metal oxide catalysts exhibit an enhanced tolerance of CO, in which the metal can disassociate water to form adsorbed OH species and then react with adsorbed CO to generate CO_2 [4]. However, during the catalyst preparation, the supporting material and its surface condition are also indispensable to achieve a high catalytic activity and decrease the amount of Pt [5,6]. In past decades, carbon-related materials are considered to be one of the most suitable catalyst supports [7–12]. Although carbon black has been widely used in the preparation of oxygen cathode or hydrogen anode [7], the appearance of novel carbon materials including carbon nanotubes [8], carbon nanofibers [9], fullerenes [10], carbon nanorods [11] and carbon nanospheres [12] have provided new candidates for carbon supports. Compared with the high temperature (up to 800 °C) and high pressure (up to 100 MPa) in carbon nanofiber synthesis and the expensive equipment in carbon nanotube fabrication, carbon nanospheres which can be easily prepared from hydrothermal synthesis of biomass have attracted more attention for their high carbon efficiency under mild conditions (<200 °C). Furthermore, biomass, its starting material, possesses intrinsic properties such as low value, huge amount, rapid generation, easy access and environmental friendship [13,14].

While choosing an electrocatalyst support, factors like electrical conductivity, surface area, macro-morphology and microstructure are considered. Usually, Pt nanoparticles are deposited on the support using reduction reagents such as sodium borohydride ($NaBH_4$) and ethylene glycol. Therefore, there is a need to find supporting materials with high surface to distribute efficiently catalyst particles and many efforts have been made in the modification of suitable supports. Especially, conducting polymers such as polypyrrole [15], polyaniline [16] and poly(arylene sulfone) [17] have been prepared with carbon nanotubes as nanocomposites and served as supporting materials. However, these polymers only provide the supporting sites of nanoparticles, and there is no positive interaction between nanoparticles and the base. To achieve a higher dispersion of nanoparticles, the supporting materials can be modified with more functional groups to anchor combined Pt, followed by a reduction step.

* Corresponding author. Tel.: +86 020 85280325; fax: +86 020 85282366.
E-mail address: liuyingju@hotmail.com (Y. Liu).

0378-7753/$ – see front matter © 2011 Elsevier B.V. All rights reserved.
doi:10.1016/j.jpowsour.2011.10.112

In general, the surface of carbon nanomaterials can be modified by covalent attachment of functional groups or non-covalent adsorption of various functional molecules. Chemical modification is the most common method to introduce the linkers, as well as to improve the efficiency and uniform deposition. Dendrimers are a novel class of highly branched and monodispersed macromolecules with well-defined composition and construction [18]. The unique properties of dendrimers, especially poly(amidoamine) (PAMAM) dendrimers, feature interior amine and amide groups that can interact with metal ion precursors through coordination chemistry or ligand exchange reaction [19]. The synthesis usually begins with the complexation of the metal precursor with PAMAM in aqueous solution, followed by the deposition of PAMAM-metal complex onto a porous catalyst with a reducing agent. Thus PAMAM has been used as a protecting ligand for the synthesis of dendrimer-entrapped [20], dendrimer-stabilized [21] or dendrimer-assembled [22] inorganic nanoparticles. Recent reports have also revealed that dendrimers can be covalently functionalized on the surface of carbon nanotubes for subsequent metal or metal oxide nanoparticle synthesis [23], which implies that by combining the dendrimers' surface functionality and unique molecular recognition ability with the electronic properties of carbon nanomaterials, it may be possible to generate various composite nanodevices for wide application in biosensor, biomedicine and bioenergy.

In this work, carbon nanospheres were prepared from glucose by a simple hydrothermal method, followed by a high temperature of calcination. After sulfuric acid treatment, the carboxyl residues on the surface of carbon nanospheres allow the conjugation with the amino groups of PAMAM dendrimers via N-(3-dimethylaminopropyl)-N′-ethylcarbodiimide hydrochloride (EDC) coupling chemistry. The remaining amino groups on the PAMAM dendrimers can be successfully employed for anchoring H_2PtCl_6 on carbon nanospheres. With the aid of $NaBH_4$, Pt nanoparticles were successfully deposited on the nanospheres. This composite material was characterized by transmission electron microscopy (TEM), X-ray photoelectron spectroscopy (XPS) and infrared spectroscopy (IR). The electrocatalytic properties of the as-prepared catalysts for methanol electrooxidation were investigated by standard electrochemical methods, revealing that Pt/PAMAM/carbon nanospheres exhibited excellent electrocatalytic activity for methanol oxidation.

2. Experimental

2.1. Chemicals

H_2PtCl_6 was purchased from China Pharmaceutical Group. $NaBH_4$ and EDC were purchased from J&K Chemical Company. Nafion solution (5%) was purchased from Dupont Company. PAMAM dendrimers were synthesized from a tetrafunctional core of ethylenediamine by successive additions of methyl acrylate and ethylenediamine following the previous method [24] and identified by ^{1}H NMR and IR. Especially, G2.0 PAMAM with 16 amino groups per molecule was used in this work. In its IR spectrum, a wide and strong peak between 3450 and 3225 cm^{-1} were due to the stretching vibration of amino groups in the compound. In addition, the peaks at 2950 cm^{-1} and 2850 cm^{-1} were ascribed to asymmetric and symmetric stretching vibrations of methylene groups, while the peaks at 1740, 1650 and 1200 cm^{-1} were stretching vibrations of carbonyl, amide and ester groups, respectively. ^{1}H NMR δ (ppm): 7.25 (–CONH–), 3.28 (CH_2NH–), 2.75 (–N(CH_2–)$_2$), 2.35 (–CH_2N–), 2.12 (–CH_2CO–), 1.6 (–NH_2) [25]. The relatively small number of resonances was a consequence of the high symmetry of the molecule and the corresponding overlap of signals [26].

2.2. Characterization

The morphology of the catalysts was monitored using TEM (Netherlands FEI) and FT-IR spectra were recorded in the range of 4000–400 cm^{-1} on a Spectrometer (VERTEX 70, Bruker, German) in the Analytical Center at South China Agriculture University. Ultra-violet spectrum was performed via a ultra-violet spectrophotometer (Shimadzu, UV 2550). The XPS spectra of the catalysts were characterized by X-ray photoelectron spectroscopy/ESCA (ESCALAB 250, Thermo Fisher Scientific Company) in the Instrumental Analysis & Research Center of Sun Yat-Sen University (Guangzhou). A monochromatic Al Ka X-ray source (1486.6 eV) was used at 15 kV and 150 W, along with pressures in the analysis chamber of about 2×10^{-7} Pa. Binding energies were referred to the C 1s peak from the carbon surface deposit at 284.8 eV.

2.3. Catalyst preparation

A volume (15 mL) of glucose at a certain concentration was placed in a 20 mL Teflon-sealed autoclave and maintained at 180 °C for 4 h. After cooling, the brown products were isolated by centrifugation, cleaned by three cycles of centrifugation/washing/redispersion in water and alcohol, and over-dried at 80 °C for 6 h. The powder was recorded as non-activated carbon spheres (NACS). Subsequently, the dried powder was calcined at 900 °C for 2 h in a N_2-permeated tube furnace at a temperature increase rate of 5 °C min^{-1}, followed by slow cooling to room temperature. Carbon spheres were finally obtained with a higher amount of carboxyl groups (ACS).

The procedure used to fabricate Pt-coated dendrimers-modified carbon spheres was as follows. In a typical synthesis, 20 mg of the above carbon spheres were immersed in 15 mL 0.5 M H_2SO_4 overnight, followed by 2 cycles of centrifugation/redispersion in water. Then, carbon spheres were dispersed in 12 mL of water, followed by the addition of EDC (10 mg). The mixture was allowed to react for 3 h under vigorous magnetic stirring, and then certain volumes of 2.5 mM PAMAM were added. The reaction was continued for another 24 h under vigorous magnetic stirring, followed by 2 cycles of centrifugation/redispersion in water to remove excess reactants. Afterwards, this powder and appropriate amounts of H_2PtCl_6 were dispersed in 20 mL water to prepare a homogeneous suspension by 60 min of ultrasonic treatment. A freshly prepared $NaBH_4$ solution was added dropwise into the above mixture under vigorous stirring. After 30 min, the product was collected by centrifugation and washed. Therefore, the composite catalyst was finally obtained after drying in a vacuum oven at 70 °C overnight (denoted as Pt/PAMAM/ACS). For comparison, the Pt/PAMAM/NACS catalyst was prepared similar to Pt/PAMAM/ACS except for using NACS instead of ACS. To investigate the role of PAMAM on methanol electrooxidation, the same procedure was used to prepare Pt directly supported on ACS and NACS (denoted as Pt/ACS and Pt/NACS).

2.4. Electrochemical characterization of the electrocatalysts

Electrochemical experiments were performed in a typical three-electrode cell using an electrochemical work station (CHI 660 C, Shanghai Chenhua Instrument). A Pt foil and a saturated calomel electrode (SCE) were used as the counter and reference electrode, respectively. All potentials in the text were referred to this reference electrode. The working electrode was prepared by depositing a thin-layer of the electrocatalyst over a glassy carbon disk (GC, 2 mm diameter) as follows: (1) a mixture containing 4.0 mg electrocatalyst and 1 ml ethanol was ultrasonically dispersed for 15 min to obtain a well-dispersed ink; (2) 5 μL of the suspension was then deposited onto a cleaned GC and dried at room temperature;

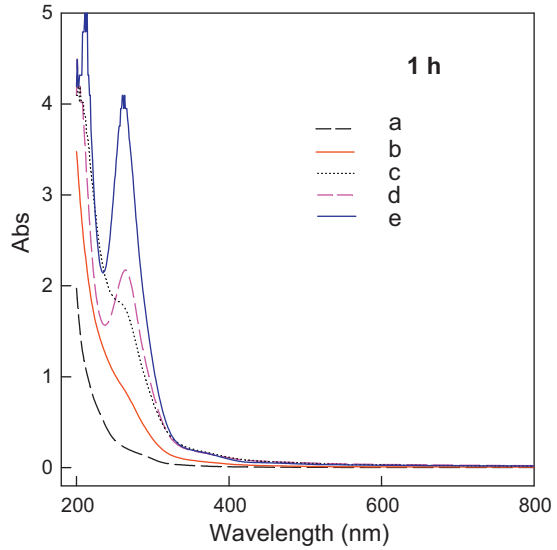

Fig. 1. The ultra-violet spectrum of H_2PtCl_6/PAMAM after 1 h mixing at different molar ratios of H_2PtCl_6 and PAMAM: (a) 10:1; (b) 20:1; (c) 30:1; (d) 40:1 and (e) 50:1.

(3) subsequently, 5 μL of 0.5% Nafion solution was added as a binder to firmly affix the electrocatalysts on the GC and the solvent was allowed to slowly evaporate. A loading mass of 3.1 μg metal nanoparticles for catalysts supported on the electrode was used.

Before the electrochemical experiment, the solution was purged with N_2 for 10 min to remove any dissolved oxygen. Methanol oxidation were characterized by cyclic voltammetry (CV) and chronoamperometry (CA) tests at room temperature. CVs were recorded in 0.1 M H_2SO_4 solution containing 2 M methanol between −0.2 and 1.0 V with a scan rate of 50 mV s^{-1}, while CA was conducted for 1 h at 0.7 V in a mixture of 0.1 M H_2SO_4 and 2 M methanol at room temperature. The CO stripping voltammetry was performed as follows. Before CO was adsorbed, the solution was purged with N_2 gas for 10 min. Then, the catalysts were held at −0.2 V in CO-saturated solution for 15 min to form a saturated CO monolayer. After the excess CO dissolved in solution was further purged out with N_2 for 15 min, the CO stripping voltammetry was performed in the potential range of −0.2 to 1.0 V with a scan rate of 10 mV s^{-1} in 0.5 M H_2SO_4.

3. Results and discussion

3.1. Optimization of reaction conditions of PAMAM and H_2PtCl_6

In the preparation of the catalysts, the complexation of Pt precursors (H_2PtCl_6) with PAMAM was involved. Therefore, the following influence factors including the molar ratio of H_2PtCl_6 with PAMAM, the incubation time of H_2PtCl_6 with PAMAM, the pH value of the solution and the ratio of $NaBH_4/H_2PtCl_6$ were discussed in detail.

Firstly, different molar ratios of H_2PtCl_6 and PAMAM were mixed in 20 mL water as 10:1, 20:1, 30:1, 40:1 and 50:1. After stirring for 1 h, UV–visible spectra were recorded to characterize the binding of H_2PtCl_6 and PAMAM. As shown in Fig. 1, if the ratio was lower than 30:1, no obvious adsorption peak can be found, suggesting an incomplete association of H_2PtCl_6 and PAMAM. However, if the ratio was higher than 40:1, an obvious peak can be discovered. Therefore, in the following experiments, the molar ratio was controlled at 40:1, which is higher than the theoretical ratio of H_2PtCl_6 and amino groups, suggesting H_2PtCl_6 can enter the cavity of PAMAM molecule [27].

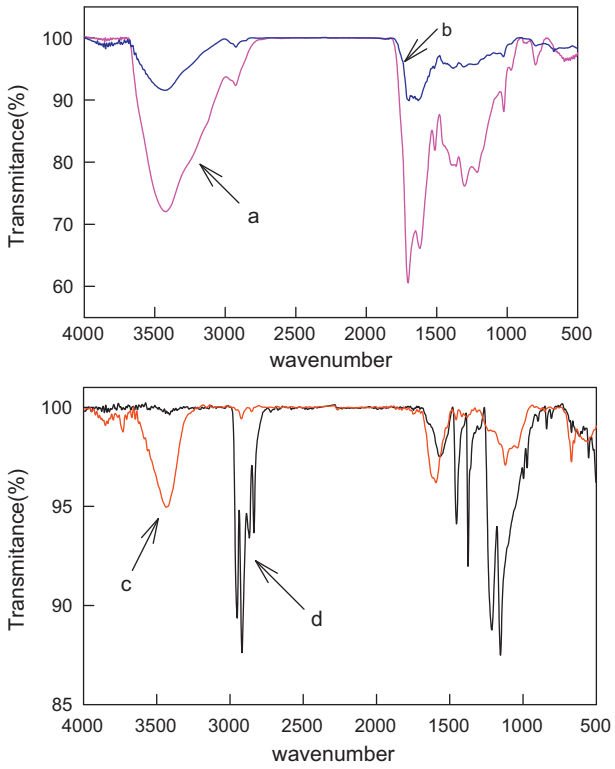

Fig. 2. The IR spectrum of NACS (a), PAMAM/NACS (b), ACS (c) and PAMAM/ACS (d).

Secondly, the influence of the incubation time of H_2PtCl_6/PAMAM mixture was monitored. If the time was 0.5 h (Supporting Fig. 1A), the adsorption peaks were all discovered at different molar ratios, which meant that the binding of H_2PtCl_6 with PAMAM was incomplete. However, if the time was 3 h, the adsorption peak can be found at the molar ratio of 40:1 and 50:1 (Supporting Fig. 1B), while the adsorption peak can only be found at a higher molar ratio than 40:1 (Supporting Fig. 1C) if the time was 5 h. Therefore, the mixing time of 1 h was selected as the optimum time.

Thirdly, the influence of the pH was studied in detail at 1, 3, 5, 7 and 9. As shown in Supporting Fig. 1D, if the pH was lower than 7, the solutions were all transparent and the adsorption peak decreased with the increase in pH. At lower pH, the protonation of amino groups will make the complexation more difficult, leading to a higher adsorption. However, if the pH was higher than 7, the precipitate will be found due to the instability of H_2PtCl_6 in basic solution. Thus, pH was selected as 5.

Finally, the molar ratio of $NaBH_4/H_2PtCl_6$ was investigated as 10:1, 20:1 and 30:1, in which the adsorption peak of H_2PtCl_6 disappeared immediately even if a molar ratio of 10:1 was selected. To ensure the completeness of the reduction, a molar ratio of 20:1 was selected.

3.2. Characterization of the as-prepared products

To confirm PAMAM immobilization on the surface of carbon nanospheres, the supporting materials were characterized by FT-IR spectroscopy and the results were shown in Fig. 2 as for NACS (Curve a), the peak at 3500 cm^{-1} was assigned to the stretching vibration of hydroxyl group, while the peak at 1700 cm^{-1} was due to the stretching vibration of carbonyl group. After its association with PAMAM (Curve b), the strength decrease of hydroxyl group and a little movement of carbonyl group were found. In IR spectrum for ACS (Curve c), the peak at 3500 and 1700 cm^{-1} can also be

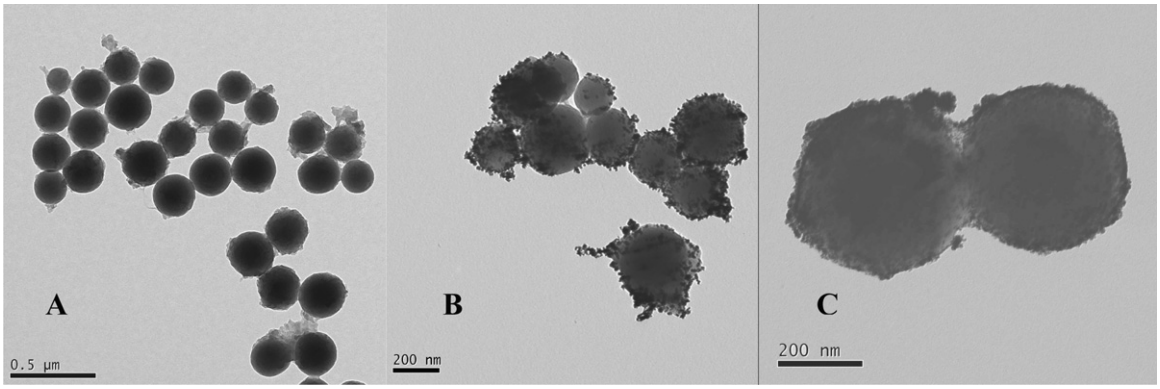

Fig. 3. TEM of ACS (A), Pt/ACS (B) and Pt/PAMAM/ACS (C).

discovered. However, after its association with PAMAM (Curve d), the peak at 3500 cm^{-1} was greatly decreased, while a much more movement of 1700 cm^{-1} was discovered. Furthermore, the peaks at 2930 and 1400 cm^{-1} were ascribed to the stretching and deforming vibration of methylene, further proving a combination of PAMAM with ACS.

The structure and morphology of the as-prepared catalysts were investigated by TEM. As shown in Fig. 3A, the TEM observation revealed that carbon products consisted of spherical microstructures with a diameter of around 250 nm, while dark particles of platinum were clearly distinguished from the carbon support for the Pt/ACS catalyst (Fig. 3B) and the Pt/PAMAM/ACS catalyst (Fig. 3C). Furthermore, compared with the Pt/ACS catalyst, the distribution of Pt nanoparticles was more uniform and the diameter of Pt nanoparticles was smaller on the Pt/PAMAM/ACS catalyst.

XPS can be used to get the information of the elements in different chemical neighborhoods on the catalyst surface. The peak position was calibrated to the C 1s peak at 284.8 eV. As shown in Fig. 4A, C, O, Pt, N can be found in the XPS survey spectrum of the Pt/PAMAM/ACS catalyst. Table 1 was XPS result for Pt/PAMAM/NACS, Pt/ACS and Pt/PAMAM/ACS, showing that the contents of Pt and N of the Pt/PAMAM/ACS catalyst were much higher than those on the Pt/PAMAM/NACS catalyst and the Pt/ACS catalyst. The reason may be that the association of activated carbon nanospheres with PAMAM was much stronger, leading to a stronger interaction with H_2PtCl_6 and a higher amount of Pt.

In Fig. 4B, Pt 4f region of the Pt/PAMAM/ACS catalyst exhibited a broad band that can be deconvolved into two pairs of doublets, both of which had a spin-orbit splitting of $4f_{7/2}$ and $4f_{5/2}$ states of ca. 3.35 eV and relative peak area close to the expected ratio of

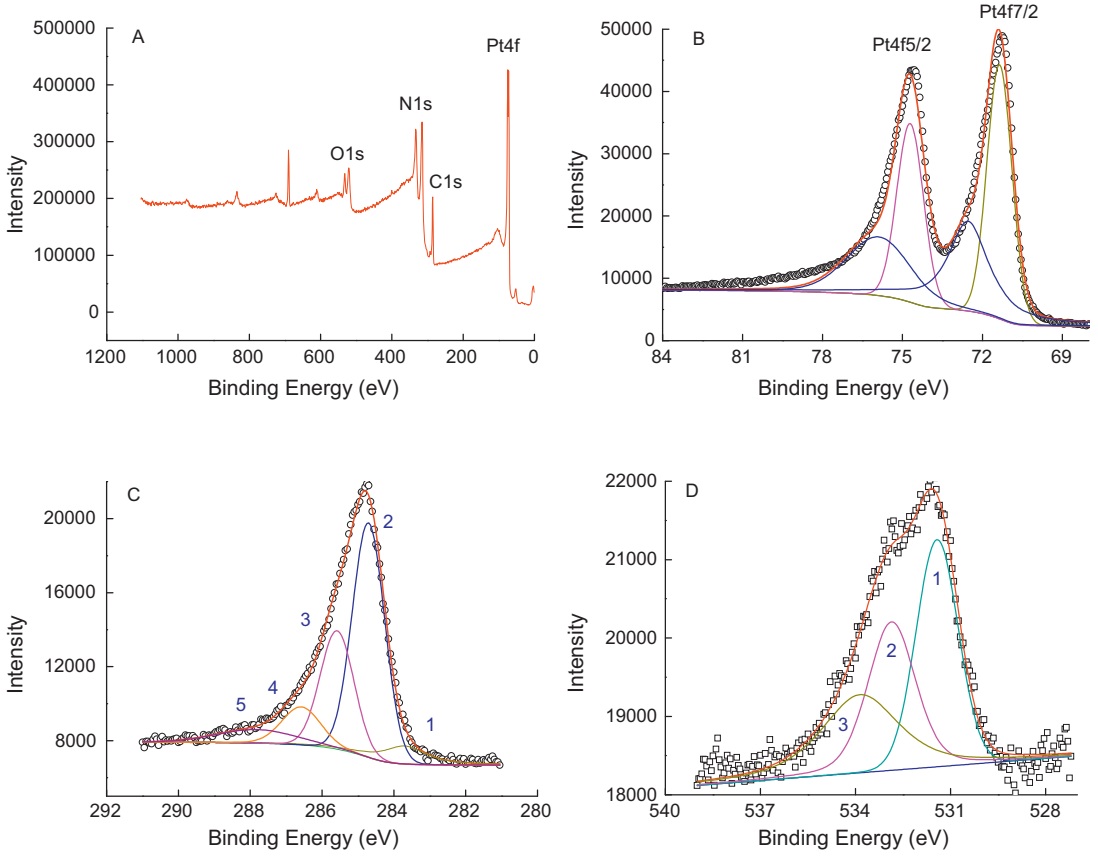

Fig. 4. XPS survey spectra of Pt/PAMAM/ACS (A), and curve deconvolution of Pt 4f (B), C 1s (C) and O 1s (D).

Table 1
XPS results of different catalysts.

Material	C (%)	O (%)	N (%)	Pt (%)	Pt (0)$4f_{7/2}$	Pt (0)$4f_{5/2}$	Pt (II)$4f_{7/2}$	Pt (II)$4f_{5/2}$
Pt/PAMAM/NACS	86.43	6.59	5.47	0.73	71.59	74.94	72.84	76.19
Pt/ACS	85.46	8.16	2.30	4.07	71.46	74.81	72.64	75.99
Pt/PAMAM/ACS	58.12	9.49	14.53	14.86	71.36	74.71	72.54	75.89

4:3. The more intense doublet peaks at 71.36 eV and 74.71 eV were attributed to metallic Pt [28], while the second and weaker doublet at 72.54 eV and 75.89 eV with higher binding energy of 1.1 eV than that of Pt^0 could be assigned to Pt (II) species due to surface oxide (PtO) or hydroxide ($Pt(OH)_2$) [29]. In addition, as shown in Table 1, the deposition of Pt on the Pt/PAMAM/ACS support slightly shifted the binding energy of Pt 4f to a lower value than that on Pt/ACS and Pt/PAMAM/NACS. For example, the binding energy of Pt $4f_{7/2}$ was 71.46 eV and 71.59 eV for metallic Pt species, respectively, indicating an interaction between Pt nanoparticles and PAMAM/ACS support [30].

Furthermore, as shown in Fig. 4C, the C 1s spectrum of the Pt/PAMAM/ACS catalyst can be also resolved into five individual component peaks, representing carbidic carbon (Peak 1, 283.7 eV), graphitic carbon (Peak 2, 284.6 eV), carbon present in alcohol or ether groups (Peak 3, 285.6 eV), carbonyl groups (Peak 4, 287.4 eV), carboxyl or ester groups (Peak 5, 289.0 eV). From the C 1s peak, the content for O-containing components accounted for a high content of the total C 1s intensity (26.1% C–OH; 10.1% C=O and 7.3% O–C=O), meaning that approximately 43% of C atoms on the surface bound with O atoms [31]. The high resolution of O 1 s spectrum (Fig. 4D) showed three peaks corresponding to C=O group (Peak 1, 531.4 eV), C–OH or C–O–C groups (Peak 2, 532.8 eV) and chemisorbed oxygen or water (Peak 3, 533.8 eV). From the O 1 s peak, the percentages for these three peaks were 38.0%, 31.4%, 30.6%, respectively, suggesting that the combination of O atoms with C atoms (about 69.4%) was the predominant existing state.

3.3. Electrochemical study

The electrochemically active surface area (ECSA) is a very important influence factor for the fuel cell reaction and the utilization ratio of Pt is closely interrelated with ECSA. Consequently, after the catalysts were immobilized on the electrode surface, ECSAs of different catalysts were detected by CVs in 0.5 M H_2SO_4 at a scan rate of 50 mV s^{-1}. As shown in curve a of Fig. 5, CV of Pt/PAMAM/ACS electrode, typical redox peaks at about 0 V were ascribed to hydrogen adsorption/desorption events at the electrode, while the small peak at 0.79 V was corresponding to the formation of platinum oxide and its related reduction peak was observed at about 0.41 V [5]. The ECSA of Pt nanoparticles for the catalyst can be signified by the integrated charge (Q_H) in the hydrogen adsorption region of the CV as the following equation [32]:

$$\text{ECSA}\ [\text{cm}^2\ \text{g}^{-1}\ \text{of Pt}] = \frac{\text{charge}\,[Q_H,\ \mu\text{C cm}^{-2}]}{210\,[\mu\text{C cm}^{-2}] \times \text{electrode loading}\,[\text{g of Pt cm}^{-2}]} \quad (1)$$

Therefore, ECSA of the Pt/PAMAM/ACS catalyst (curve a) can be calculated as 65.93 $m^2\ g^{-1}$, much higher than that on the Pt/ACS catalyst (curve e, 15.80 $m^2\ g^{-1}$), indicating PAMAM modification on carbon nanospheres caused a higher Pt immobilization by the association of PAMAM and H_2PtCl_6. The inset figure was Pt nanoparticles directly depositing on carbon nanospheres without calcination at a high temperature, in which curve f and curve g were Pt/PAMAM/NACS (6.85 $m^2\ g^{-1}$) and Pt/NACS (5.0 $m^2\ g^{-1}$), respectively. A much higher current density indicated that this calcination can produce more carboxyl groups on the outside of carbon nanospheres, which was very similar to the treatment of carbon nanotubes by concentrated sulfuric acid and nitric acid in earlier reports [23,33]. Furthermore, the influence of glucose concentration was also investigated and CVs were depicted in curve b–d. The current density gradually decreased at a higher glucose concentration, in which ECSAs were 38.22 $m^2\ g^{-1}$, 33.44 $m^2\ g^{-1}$ and 16.72 $m^2\ g^{-1}$ for 0.8, 0.9 and 1.0 M glucose, respectively, resulting from different diameters and different specific surface areas of these nanospheres from different concentrations [14,34].

Electrochemical oxidation of methanol has also gained importance in energy conversion in the form of DMFCs. Consequently, methanol electrooxidation at the Pt/PAMAM/ACS catalyst was investigated by cyclic voltammetry. As shown in Fig. 6, the voltammograms were similar to those reported in the literature [7,15], with two irreversible current peaks during the electrooxidation of methanol, typically attributing to methanol electrooxidation (forward scan peak at around 0.65 V) and the re-oxidation of methanol (backward peak at 0.45 V) due to the reduction of platinum oxide [35]. The onset potential of methanol oxidation on the Pt/PAMAM/ACS (curve a) was 0.12 V, which was lower than that for the Pt/ACS (curve e, 0.19 V), Pt/PAMAM/NACS (curve f, 0.34 V) and Pt/NACS (curve g, 0.40 V) [36]. Furthermore, the peak current density of methanol oxidation at the first scan on these four catalysts had following order: Pt/PAMAM/ACS (369 mA mg^{-1}) > Pt/ACS (78 mA mg^{-1}) > Pt/PAMAM/NACS (5.8 mA mg^{-1}) > Pt/NACS (2.0 mA mg^{-1}), indicating the Pt/PAMAM/ACS catalyst gave the highest peak current density, which was similar to ECSA test. With the same Pt loading, the current density of Pt/PAMAM/ACS catalyst was 4.7, 64, and 184 times that of Pt/ACS, Pt/PAMAM/NACS and Pt/NACS, respectively. Two reasons can be found: firstly, the activation of carbon spheres at high temperature produced more carboxyl groups, which made the surface more rough and a higher accessible surface area, leading to better Pt dispersion and immobilization on its surface;

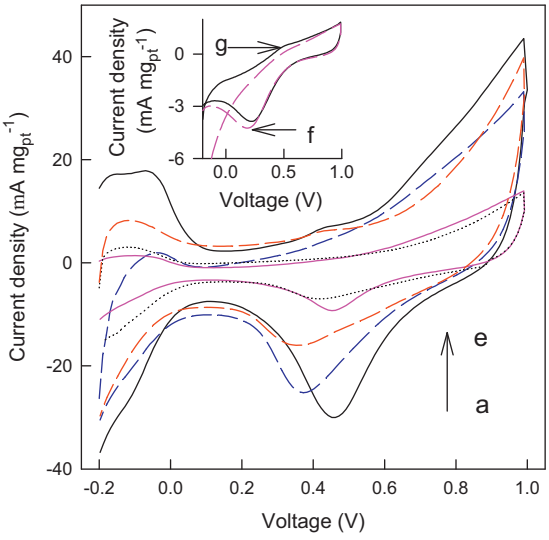

Fig. 5. CVs of Pt/PAMAM/ACS of carbon nanospheres from (a) 0.7 M, (b) 0.8 M, (c) 0.9 M, (d) 1.0 M glucose, and Pt/ACS (e), Pt/PAMAM/NACS (f) and Pt/NACS (g) of carbon nanospheres from 0.9 M glucose in 0.5 M H_2SO_4 at a scan rate of 50 mV s^{-1}.

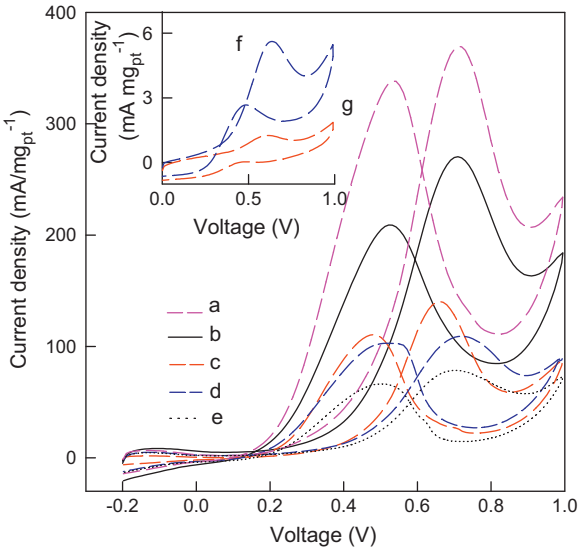

Fig. 6. CVs of Pt/PAMAM/ACS of carbon nanospheres from (a) 0.7 M, (b) 0.8 M, (c) 0.9 M, (d) 1.0 M glucose, and Pt/ACS (e), Pt/PAMAM/NACS (f) and Pt/NACS (g) of carbon nanospheres from 0.9 M glucose in 0.1 M H_2SO_4 + 2 M methanol at a scan rate of 50 mV s^{-1}.

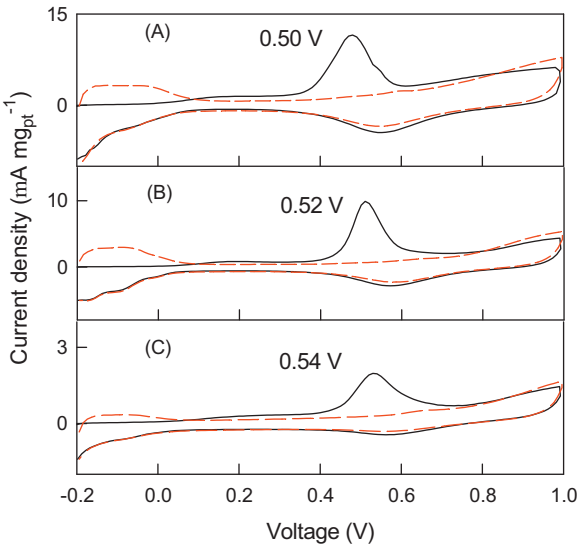

Fig. 8. CO stripping voltammograms in 0.5 M H_2SO_4 at Pt/PAMAM/ACS (A), Pt/ACS (B) and Pt/NACS (C) at a scan rate of 10 mV s^{-1}.

secondly, these carboxyl groups can associate with PAMAM, which can chelate with more Pt^{4+} using their amino groups conveniently and enhance the loading of Pt nanoparticles. In addition, the peak current density of methanol oxidation at the Pt/PAMAM/ACS catalyst decreased with the increase in glucose concentrations. The maximum value of the peak current density was found for carbon spheres from 0.7 M glucose, which was coincided with ECSA detection. Moreover, the onset potentials of methanol oxidation on the Pt/PAMAM/ACS were 0.13 V, 0.15 V and 0.17 V for carbon spheres prepared from 0.8 M, (curve b), 0.9 M (curve c) and 1.0 M (curve d) glucose, respectively.

In order to compare the long-term performance of the catalysts toward methanol oxidation, the typical current density–time response of Pt-based catalysts for methanol was recorded with time at a fixed potential of 0.7 V. As in Fig. 7, the current gradually decayed with time for all the catalysts due to the formation of intermediate species, such as CO_{ads}, CHO_{ads} and CH_3O_{ads}, during the methanol reaction [37]. However, the decay in the oxidation current with time was different. As expected, the methanol oxidation current density at Pt/PAMAM/ACS (curve a) was evidently higher after long-time operation than that at Pt/ACS (curve d), Pt/PAMAM/NACS (curve e) and Pt/NACS (curve f), illustrating that this catalyst exhibited more excellent stability and higher catalytic activity for methanol oxidation, which was in agreement with cyclic voltammograms. Moreover, the long-time stability for the catalysts prepared from 0.8 M (curve b), 0.9 M (curve c) and 1.0 M (curve d) were monitored. It is well-known that different sizes of carbon nanospheres can be obtained from different concentrations of glucose, which can finally influence the stability of the nanocomposites [13,14].

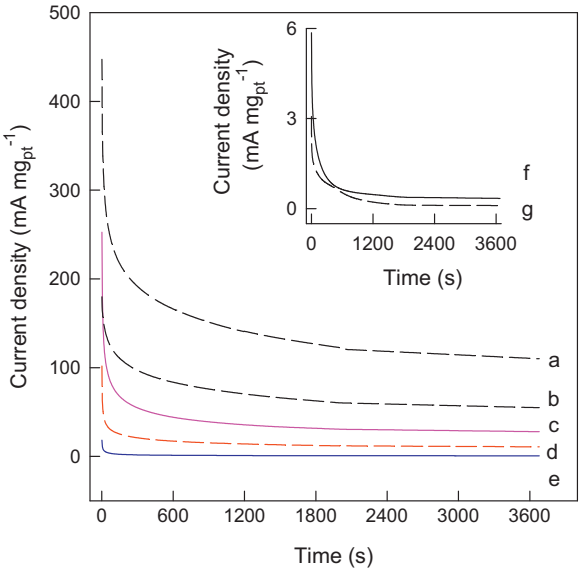

Fig. 7. Chronoamperometric curves of Pt/PAMAM/ACS of carbon nanospheres from (a) 0.7 M, (b) 0.8 M, (c) 0.9 M, (d) 1.0 M glucose, and Pt/ACS (e), Pt/PAMAM/NACS (f) and Pt/NACS (g) of carbon nanospheres from 0.9 M glucose in 0.1 M H_2SO_4 + 2 M methanol at a constant potential of 0.7 V.

The tolerance ability for CO poison also influences the catalytic properties of the catalysts. If a catalyst has a higher ability to CO oxidation, it can oxidize more CO or oxidize CO at lower potential [38]. Fig. 8 showed the CO-stripping voltammograms for different Pt based catalysts. It can be seen that prior to the oxidation of adsorbed CO, the hydrogen adsorption/desorption was completely suppressed in all curves (the red line); but the peak associated with hydrogen adsorption appeared after the removal of adsorbed CO (the black line). The peak potential for CO oxidation on the Pt/PAMAM/ACS (A) catalyst was negatively shifted to 0.50 V, while the potentials were 0.52 V and 0.54 V on the Pt/ACS (B) and Pt/NACS (C) catalyst, respectively, indicating that the pre-adsorbed CO was easier to be oxidized on the PAMAM/ACS. The reaction scheme for the CO electrochemical oxidation on Pt was as following [39]:

$$H_2O + Pt \rightarrow Pt\text{–}OH_{ads} + H^+ + e^- \quad (2)$$

$$Pt\text{–}CO_{ads} + Pt\text{–}OH_{ads} \rightarrow CO_2 + H^+ + e^- + Pt \quad (3)$$

The surface mobility of CO_{ads} and OH_{ads} significantly influenced the electrochemical CO oxidation. In the former XPS data, the Pt/PAMAM/ACS catalyst had a weaker binding energy with oxygen-containing species than Pt/ACS, which would improve the mobility of CO_{ads} and OH_{ads}. Therefore, the diffusion or intermixing of CO_{ads} and OH_{ads} was much easier on Pt/PAMAM/ACS, resulting in the fast electrooxidation of CO_{ads}.

4. Conclusion

We have prepared Pt/PAMAM/ACS nanocomposites by covalent immobilization of carbon nanospheres with PAMAM, and in situ chemical reduction of chloroplatinic acid. The structures of the nanocomposites were characterized by TEM, FT-IR and XPS, which revealed that a higher temperature of calcination can improve the amount of oxygen-containing groups on carbon nanospheres and the interaction can be found between carbon spheres with PAMAM. The study of the electrocatalytic activity of the platinized-catalyst for methanol oxidation indicated that Pt/PAMAM/ACS possessed higher catalytic response, stability and CO tolerance than other catalysts, a demonstration that the chelation of carboxyl groups with PAMAM increased the Pt loading on the surface. The use of PAMAM in combination nanoparticles may provide a method for the catalytic enhancement of high-performance anodes for DMFC.

Acknowledgements

The authors thank for Dr. Javier Ramón-Azcón in WPI Advanced Institute for Materials Research, Tohoku University, Japan for English edition and the financial support of Natural Science Foundation of China (21105030, 20827006), the National Basic Research Program of China (2009CB421601), the Student Innovative Project of Guangdong Province (1056411139) and the Key Academic Program of 211 Project of South China Agricultural University (2009B010100001).

Appendix A. Supplementary data

Supplementary data associated with this article can be found, in the online version, at doi:10.1016/j.jpowsour.2011.10.112.

References

[1] A.S. Aricò, S. Srinivasan, V. Antonucci, Fuel Cells 1 (2001) 33–161.
[2] C. Alegre, L. Calvillo, R. Moliner, J.A. González-Expósito, O. Guillén-Villafuerte, M.V.M. Huerta, E. Pastor, M.J. Lázaro, J. Power Sources 196 (2011) 4226–4235.
[3] M. Zhiani, B. Rezaei, J. Jalili, Int. J. Hydrogen Energy 35 (2010) 9298–9305.
[4] D.J. Guo, X.P. Qiu, W.T. Zhu, L.Q. Chen, Appl. Catal. B: Environ. 89 (2009) 597–601.
[5] L. Xing, J.B. Jia, Y.Z. Wang, B.L. Zhang, S.J. Dong, Int. J. Hydrogen Energy 35 (2010) 12169–12173.
[6] H.Q. Song, X.P. Qiu, F.S. Li, Appl. Catal. A Gen. 364 (2009) 1–7.
[7] R.F. Wang, H. Wang, B.X. Wei, W. Wang, Z.Q. Lei, Int. J. Hydrogen Energy 35 (2010) 10081–10086.
[8] R. Ahmadi, M.K. Amini, Int. J. Hydrogen Energy 36 (2011) 7275–7283.
[9] Z. Lin, L.W. Ji, X.W. Zhang, Electrochim. Acta 54 (2009) 7042–7047.
[10] J.J. Guo, X.W. Yang, Y.L. Yao, X.M. Wang, X.G. Liu, B.S. Xu, Rare Metals 25 (2006) 305–308.
[11] J.H. Nam, Y.Y. Jang, Y.U. Kwon, J.D. Nam, Electrochem. Commun. 6 (2004) 737–741.
[12] X. Wang, C.G. Hu, Y.F. Xiong, H. Liu, G.J. Du, X.S. He, J. Power Sources 196 (2011) 1904–1908.
[13] B. Hu, S.H. Yu, K. Wang, L. Liu, X.W. Xu, Dalton Trans. 40 (2008) 5414–5423.
[14] M. Sevilla, A.B. Fuertes, Chem. Eur. J. 15 (2009) 4195–4203.
[15] B. Qu, Y.T. Xu, S.J. Lin, Y.F. Zheng, L.Z. Dai, Synth. Met. 160 (2010) 732–742.
[16] S. Lefrant, M. Baibarac, I. Baltog, C. Godon, J.Y. Mevellec, J. Wéry, E. Faulques, L. Mihut, H. Aarab, O. Chauvet, Synth. Met. 155 (2005) 666–669.
[17] S.H. Joo, C. Pak, E.A. Kim, Y.H. Lee, H. Chang, D. Seung, Y.S. Choi, J. Park, T.K. Kim, J. Power Sources 180 (2008) 63–70.
[18] M. Giannetto, L. Mori, G. Mori, M. Careri, A. Mangia, Sens. Actuat. B: Chem. 159 (2011) 185–192.
[19] Y.L. Gu, G. Wu, X.F. Hu, D.A. Chen, T.J. Hansen, H. zur Loye, H.J. Ploehn, J. Power Sources 195 (2010) 425–434.
[20] X. Shi, I. Lee, J.R. Baker Jr., J. Mater. Chem. 18 (2008) 586–593.
[21] W. Lesniak, A.U. Bielinska, K. Sun, K.W. Janczak, X. Shi, J.R. Baker Jr., L.P. Balogh, Nano. Lett. 5 (2005) 2123–2130.
[22] X.Y. Shi, S.H. Wang, S.D. Swanson, S. Ge, Z. Cao, M.E. Van Antwerp, K.J. Landmark, J.R. Baker Jr., Adv. Mater. 20 (2008) 1671–1678.
[23] X.Y. Shi, S.H. Wang, M.W. Shen, M.E. Van Antwerp, X.S. Chen, C. Li, E.J. Petersen, Q.G. Huang, W.J. Weber Jr., J.R. Baker Jr., Biomacromolecules 10 (2009) 1744–1750.
[24] B. Devarakonda, R.A. Hill, M.M. de Villiers, Int. J. Pharm. 284 (2004) 133–140.
[25] M.V. Gomez, J. Guerra, A.H. Velders, R.M. Crooks, J. Am. Chem. Soc. 131 (2009) 341–350.
[26] M.V. Gomez, J. Guerra, V.S. Myers, R.M. Crooks, A.H. Velders, J. Am. Chem. Soc. 131 (2009) 14634–14635.
[27] Y.L. Gu, P. Sanders, H.J. Ploehn, Colloids Surf. A 356 (2010) 10–15.
[28] C.H. Yen, K. Shimizu, Y.Y. Lin, F. Bailey, I.F. Cheng, C.M. Wai, Energy Fuels 21 (2007) 2268–2271.
[29] D.H. Lim, D.H. Choi, W.D. Lee, H.I. Lee, Appl. Catal. B: Environ. 89 (2009) 484–493.
[30] L. Ma, X. Zhao, F.Z. Si, C.P. Liu, J.H. Liao, L. Liang, W. Xing, Electrochim. Acta 55 (2010) 9105–9112.
[31] M. Titirici, A. Thomas, M. Antonietti, J. Mater. Chem. 17 (2007) 3412–3418.
[32] G. Girishkumar, M. Rettker, R. Underhile, D. Binz, K. Vinodgopal, P. McGinn, P. Kamat, Langmuir 21 (2005) 8487–8494.
[33] A. Kaushik, P.R. Solanki, M.K. Pandey, K. Kaneto, S. Ahmad, B.D. Malhotra, Thin Solid Films 519 (2010) 1160–1166.
[34] X.M. Sun, Y.D. Li, Angew. Chem. Int. Ed. 43 (2004) 597–601.
[35] K.L. Nagashree, N.H. Raviraj, M.F. Ahmed, Electrochim. Acta 55 (2010) 2629–2635.
[36] S.M. Choi, M.H. Seo, H.J. Kim, W.B. Kim, Carbon 49 (2011) 904–909.
[37] J.R.C. Salgado, F. Alcaide, G. Álvarez, L. Calvillo, M.J. Lázaro, E. Pastor, J. Power Sources 195 (2010) 4022–4029.
[38] G. García, J. Florez-Montaño, A. Hernandez-Creus, E. Pastor, G.A. Planes, J. Power Sources 196 (2011) 2979–2986.
[39] F. Maillard, M. Eikerling, O.V. Cherstiouk, S. Schreier, E. Savinova, U. Stimming, Faraday Discuss. 125 (2004) 357–377.